Frame-invariant formulation of novel Generalized Newtonian fluid constitutive equation for polymer melts

Martin Zatloukal*

Polymer Centre, Faculty of Technology, Tomas Bata University in Zlín,

Vavrečkova 275, 760 01 Zlín, Czech Republic

Keywords: Constitutive equation, Generalized Newtonian fluid, polymer melt, extensional rheology.

*Corresponding author: mzatloukal@utb.cz

ABSTRACT

In this work, the frame-invariant formulation of a new generalized Newtonian fluid (GNF) constitutive equation is proposed. Viscosity is given as a specific function of the second and third invariant of the strain rate tensor, and the second invariant of the objective velocity gradient. The GNF model was successfully tested using experimental data taken from the open literature for different high and low density polyethylene melts with varying amounts of long-chain branches utilizing steady-state shear, uniaxial and planar extensional viscosities plotted as a function of the strain rate.

The Generalized Newtonian Fluid (GNF) constitutive equation, in which the viscosity is allowed to vary with the second, II_D, and/or third, III_D, invariants of the strain rate tensor, *D*, [1-4] is widely used to model isotropic and incompressible complex fluid flows to improve convergence of solutions for very fast flows. The main disadvantage of the GNF model is its inability to realistically represent extensional rheology, especially in planar flows, where $\mathrm{III}_D = 0$. To overcome this problem, Zatloukal [5-7] proposed a GNF model in which the viscosity is given as a specific function of II_D, III_D and the first invariant of the absolute value of the strain rate tensor, $I_{|D|}$, characterizing overall amount of stretching during the flow (where $|\mathrm{D}| = \sqrt{\mathrm{D}\cdot\mathrm{D}}$). This model has been found to provide correct behaviour in describing steady-state shear and extensional viscosities for various polymer melts [5,7-9] and has been used successfully in modelling of the film blowing process [8, 10-11]. However, the use of the model in mixed shear and extensional flows is complicated because $I_{|D|}$ needs to be evaluated in a local, streamline oriented coordinate system to avoid multiple solutions and to keep its physical meaning [5]. In order to overcome this problem, a new modification of the GNF model is proposed here to provide a simple frame-invariant formulation of the model, maintaining its ability to describe the steady-state shear and extensional rheology of polymer melts.

To distinguish between different types of flows, we used an objective velocity gradient, $\overline{L}$, proposed by Yao [12-13], which is defined as

$$\overline{\mathrm{L}} = \mathrm{D} + \overline{\mathrm{W}} \tag{1}$$

where *D* is the strain rate tensor and $\overline{W}$ is the objective vorticity tensor defined as

$$\mathrm{D} = \frac{1}{2}\left(\mathrm{L} + \mathrm{L}^{\mathrm{T}}\right) \text{ and } \overline{\mathrm{W}} = \frac{1}{2}\left(\mathrm{L} - \mathrm{L}^{\mathrm{T}}\right) - \Omega \tag{2}$$

Here, L represents the velocity gradient tensor and Ω is the rigid part of the body subtracted from the classical vorticity tensor, which is related to the rotation of the principal axes of D [12-13]. The rigid-body vorticity Ω is defined as

$$\frac{De_i}{Dt} = \Omega \cdot e_i \tag{3}$$

where $\frac{D}{Dt}$ is the substantial time derivative and e_i (for i = 1, 2, 3) are unit vectors along the principal axes of D. When at least two of the eigenvalues of D coincide, the corresponding components in Ω must be set equal to those in W, which makes the definition of Ω in Eq. 3 unique [12, 14]. Therefore, for steady-state flow, Ω disappears and $\bar{L}$ and L becomes the same [12-13]. The GNF model, which was proposed in our previous work [5-7], is modified here by replacing the absolute value of the strain rate tensor, $|D|$, (defined as $\sqrt{D \cdot D}$) with the objective velocity gradient, $\bar{L}$. The modified GNF model has the following form

$$\tau = 2\eta\left(\mathrm{II}_{\bar{L}}, \mathrm{II}_D, \mathrm{III}_D\right)D \tag{4}$$

where τ is the extra stress tensor and η is the viscosity, which is allowed to vary with the second $\mathrm{II}_{\bar{L}} = 2\mathrm{tr}\left(\bar{L}^2\right)$ invariant of $\bar{L}$ as well as with the second $\mathrm{II}_D = 2\mathrm{tr}\left(D^2\right)$, and third, $\mathrm{III}_D = \det(D)$, invariants of D according to Eq. 5

$$\eta\left(\mathrm{II}_{\bar{L}}, \mathrm{II}_D, \mathrm{III}_D\right) = A^{1-f\left(\mathrm{II}_{\bar{L}}, \mathrm{II}_D, \mathrm{III}_D\right)}\eta\left(\mathrm{II}_D\right)^{f\left(\mathrm{II}_{\bar{L}}, \mathrm{II}_D, \mathrm{III}_D\right)} \tag{5}$$

where $\eta(II_D)$ is given by Eq. 6 representing the well-known Carreau-Yasuda model and $f\left(\mathrm{II}_{\bar{L}}, \mathrm{II}_D, \mathrm{III}_D\right)$ is given by Eq. 7

$$\eta\left(\mathrm{II}_D\right) = \eta_\infty + \frac{\eta_0 - \eta_\infty}{\left[1 + \left(\lambda_1\sqrt{\mathrm{II}_D}\right)^a\right]^{\left(\frac{1-n}{a}\right)}} \tag{6}$$

$$f\left(II_{\bar{L}}, II_D, III_D\right) = \left\{ \tanh\left[\lambda_2 \left(1+\frac{1}{12\sqrt{3}}\right)^{-\psi} \left(\left| 1+\frac{III_D}{II_D^{3/2}} \right| \right)^{\psi} \sqrt{II_{\bar{L}}} + \beta \right] \frac{1}{\tanh(\beta)} \right\}^{\zeta} \tag{7}$$

where A, η_0, η_∞, λ_1, a, n, λ_2, ψ, β, ζ are 10 adjustable parameters.

The model utilizes 5 parameters (η_0, η_∞, λ_1, a, n) identifiable from shear viscosity, 4 parameters (A, λ_2, β, ζ) identifiable from uniaxial extensional viscosity and 1 parameter (ψ), which can be determined from the planar extensional viscosity. In a simple shear flow, the function $f\left(II_{\bar{L}}, II_D, III_D\right)$ defined by Eq. 7 is 1 because $\sqrt{II_{\bar{L}}} = 0$. On the other hand, in extensional flows, the term $\sqrt{II_{\bar{L}}}$ becomes nonzero (equal to $\sqrt{3}\dot{\varepsilon}$ for uniaxial flow, $2\sqrt{3}\dot{\varepsilon}$ for equibiaxial flow, and $2\dot{\varepsilon}$ for planar flow) and as a result, the function $f\left(II_{\bar{L}}, II_D, III_D\right)$ starts to deviate from 1. The adjusted value of the term $\left(1+\frac{1}{12\sqrt{3}}\right)^{-\psi}\left(\left|1+\frac{III_D}{II_D^{3/2}}\right|\right)^{\psi}$ via the parameter ψ enables independent control of planar and equibiaxial extensional viscosity, while the shear and uniaxial extensional viscosity do not change as in the original model [5-7]. The key difference between the modified GNF model and its original version is the $\sqrt{II_{\bar{L}}}$ term that appears in the function f, instead of the original $\frac{\sqrt[3]{4\left|III_D\right|}+I_{|D|}}{3}$ term. The main invariants for D and $\bar{L}$ are given in Tables 1 and 2 for simple and mixed flows. It can be seen that for pure shear and extensional flow $II_{\bar{L}}$ becomes zero and non-zero, respectively, and it depends only on the extensional strain rate, regardless of the type of mixed flow. $II_{\bar{L}}$ can therefore be considered as a variable characterizing the intensity of stretching during flow.

The modified GNF model provides analytical expressions for shear viscosity, η_S, as well as uniaxial, $\eta_{E,U}$, biaxial, $\eta_{E,B}$, and planar, $\eta_{E,P}$, extensional viscosities, which are summarized below.

$$\eta_S = \eta_\infty + \frac{\eta_0 - \eta_\infty}{\left[1+\left(\lambda_1\dot{\gamma}\right)^a\right]^{\frac{1-n}{a}}} \tag{8}$$

$$\eta_{E,U} = 3^*A^{1-\left[\tanh\left(\lambda_2\sqrt{3}\dot{\varepsilon}+\beta\right)/\tanh(\beta)\right]^\zeta}\left\{\eta_\infty + \frac{\eta_0 - \eta_\infty}{\left[1+\left(\lambda_1\sqrt{3}\dot{\varepsilon}\right)^a\right]^{\frac{1-n}{a}}}\right\}^{\left[\tanh\left(\lambda_2\sqrt{3}\dot{\varepsilon}+\beta\right)/\tanh(\beta)\right]^\zeta} \tag{9}$$

$$\eta_{E,B} = 6^*A^{1-\left\{\tanh\left[\lambda_2\left(1-\frac{2}{1+12\sqrt{3}}\right)^\psi 2\sqrt{3}\dot{\varepsilon}+\beta\right]/\tanh(\beta)\right\}^\zeta}\left\{\eta_\infty + \frac{\eta_0 - \eta_\infty}{\left[1+\left(\lambda_1 2\sqrt{3}\dot{\varepsilon}\right)^a\right]^{\frac{1-n}{a}}}\right\}^{\left\{\tanh\left[\lambda_2\left(1-\frac{2}{1+12\sqrt{3}}\right)^\psi 2\sqrt{3}\dot{\varepsilon}+\beta\right]/\tanh(\beta)\right\}^\zeta} \tag{10}$$

$$\eta_{E,P} = 4^*A^{1-\left\{\tanh\left[\lambda_2\left(1-\frac{1}{1+12\sqrt{3}}\right)^\psi 2\dot{\varepsilon}+\beta\right]/\tanh(\beta)\right\}^\zeta}\left\{\eta_\infty + \frac{\eta_0 - \eta_\infty}{\left[1+\left(\lambda_1 2\dot{\varepsilon}\right)^a\right]^{\frac{1-n}{a}}}\right\}^{\left\{\tanh\left[\lambda_2\left(1-\frac{1}{1+12\sqrt{3}}\right)^\psi 2\dot{\varepsilon}+\beta\right]/\tanh(\beta)\right\}^\zeta} \tag{11}$$

In order to test the modified GNF model, steady-state shear, uniaxial and planar extensional viscosities plotted as a function of the strain rate were used for highly branched low-density polyethylenes, LDPEs as well as metallocene high-density (mHDPE) and linear low-density (mLLDPE) polyethylenes with varying amounts of long-chain branches. Experimental data were taken from [15] and the fitting procedure was as follows. First, the shear viscosity was fitted by the Carreau-Yasuda function (Eq. 8) to determine η_0, η_∞, λ_1, a, n parameters. Second, A, λ_2, β, ζ model parameters were identified on uniaxial extensional viscosity data via Eq. 9 (keeping η_0, η_∞, λ_1, a, n parameters unchanged). Third, the remaining ψ parameter was determined by fitting the planar extensional viscosity data by Eq. 11 (keeping all other parameters fixed). In the final stage, shear, uniaxial and planar extensional viscosities were fitted simultaneously via Eqs. 8-9, 11 using the parameter values determined in previous three steps as initial values. Note that due to the absence of a secondary high strain rate plateau, the parameters η_∞ and A were fixed at 0 Pa.s and 10^{-8} Pa.s, respectively. A comparison of model fits and measured data is shown

in Figures 1-2 and the corresponding model parameters are listed in Tables 3-4. It can be seen that the modified GNF model has a very good ability to describe measured data for all polymer samples tested. The physical role of the 5 extension related parameters is as follows: λ_2, ζ and β dominantly controls the uniaxial extensional strain hardening (their values have tendency to increase with LCB, see Table 4), ψ allows independent control of steady planar/equibiaxial extensional viscosity (its increase reduces strain hardening and promotes strain thinning) and *A* parameter is related to the high-extension rate plateau value of the extensional viscosity. The model has the ability to describe lower $\eta_{E,P}$ at high strain rates compared to $\eta_{E,U}$ for highly branched LDPEs (see Figure 1) as well as a gradual decrease in $\eta_{E,P}$ relative to $\eta_{E,U}$ at high strain rates with increased level of long chain branching for mLLDPE and mHDPE polymer samples through an increased parameter ψ (see Figure 2 and Table 4). It is important to note that various widely used constitutive equations (including the molecular-based Pom–Pom model [15], see Figure S1 in supplementary material) are not able to handle these differences because they predict steady-state uniaxial and planar extensional viscosities to become virtually identical at high extensional strain rates [16], which is not realistic for the studied polymers. This suggests that the use of the modified GNF model in modeling of polymer processing can significantly help with material, equipment design and process optimization, and can provide explanations for flow phenomena that are not yet fully understood (for example vortex formation [17-18], neck-in phenomenon [16, 19-21] or instabilities in the melt blowing process [22-24], etc.).

See supplementary material for additional information, which includes a comparison between the modified GNF model fits and corresponding experimental rheological data for well-characterized branched IUPAC A LDPE and linear HDPE Liten polymer melts, which are available in a wide range of strain rates.

The author would like to acknowledge the Institutional Support Project 2020 (Polymer Centre at Faculty of Technology, Tomas Bata University in Zlin).

The data that supports the findings of this study are available within the article.

REFERENCES

1. B. Debbaut, M.J. Crochet, "Extensional effects in complex flows," Journal of Non-Newtonian Fluid Mechanics 30 (2-3), 169-184 (1988).
2. P.R. Schunk, L.E. Scriven, "Constitutive equation for modeling mixed extension and shear in polymer solution processing," Journal of Rheology 34 (7), 1085-1119 (1990).
3. W.N. Song, Z.M. Xia, "A phenomenological viscosity model for polymeric fluid," Journal of Non-Newtonian Fluid Mechanics 53 (C), 151-163 (1994).
4. H.C. Tseng, "A revisitation of generalized Newtonian fluids," Journal of Rheology 64 (3), 493-504 (2020).
5. M. Zatloukal, "A simple phenomenological non-Newtonian fluid model," Journal of Non-Newtonian Fluid Mechanics 165 (11-12), 592-595 (2010).
6. M. Zatloukal, "Novel non-Newtonian fluid model for polymer melts," Annual Technical Conference - ANTEC, Conference Proceedings, 1, 92-96 (2011).
7. M. Zatloukal, "Measurements and modeling of temperature-strain rate dependent uniaxial and planar extensional viscosities for branched LDPE polymer melt," Polymer, 104, 258-267 (2016).
8. R. Kolarik, M. Zatloukal, M. Martyn, "The effect of polyolefin extensional rheology on non-isothermal film blowing process stability," International Journal of Heat and Mass Transfer, 56 (1-2), 694-708 (2013).

9. J. Drabek, M. Zatloukal, "Evaluation of thermally induced degradation of branched polypropylene by using rheology and different constitutive equations," Polymers, 8 (9), art. no. 317 (2016).
10. R. Kolarik, M. Zatloukal, "Modeling of nonisothermal film blowing process for non-Newtonian fluids by using variational principles," Journal of Applied Polymer Science, 122 (4), 2807-2820 (2011).
11. R. Kolarik, M. Zatloukal, C. Tzoganakis, "Stability analysis of non-isothermal film blowing process for non-Newtonian fluids using variational principles," Chemical Engineering Science 73, 439-453 (2012).
12. D. Yao, "A non-Newtonian fluid model with an objective vorticity," Journal of Non-Newtonian Fluid Mechanics, 218, 99-105 (2015).
13. D. Yao, "A non-Newtonian fluid model with finite stretch and rotational recovery," Journal of Non-Newtonian Fluid Mechanics, 230, 12-18 (2016).
14. G. Astarita, "Objective and generally applicable criteria for flow classification," Journal of Non-Newtonian Fluid Mechanics, 6 (1), 69-76 (1979).
15. D. Auhl, D. M. Hoyle, D. Hassell, T. D. Lord, O. G. Harlen, M. R. Mackley, and T. C. B. McLeish, "Cross-slot extensional rheometry and the steady-state extensional response of long chain branched polymer melts," Journal of Rheology 55 (4), 875 (2011).
16. T. Barborik, M. Zatloukal, "Steady-state modeling of extrusion cast film process, neck-in phenomenon, and related experimental research: A review," Physics of Fluids 32 (6), art. no. 061302 (2020).
17. J. Musil, M. Zatloukal, "Historical Review of Secondary Entry Flows in Polymer Melt Extrusion," Polymer Reviews 59 (2), 338-390 (2019).

18. L. L. Ferrás, A. M. Afonso, M. A. Alves, J. M. Nóbrega, F. T. Pinho, "Newtonian and viscoelastic fluid flows through an abrupt 1:4 expansion with slip boundary conditions," Physics of Fluids 32, 043103 (2020).
19. T. Barborik, M. Zatloukal, "Effect of heat transfer coefficient, draw ratio, and die exit temperature on the production of flat polypropylene membranes," Physics of Fluids 31 (5), art. no. 053101 (2019).
20. T. Barborik, M. Zatloukal, "Effect of die exit stress state, Deborah number, uniaxial and planar extensional rheology on the neck-in phenomenon in polymeric flat film production," Journal of Non-Newtonian Fluid Mechanics 255, 39-56 (2018).
21. T. Barborik, M. Zatloukal, C. Tzoganakis, "On the role of extensional rheology and Deborah number on the neck-in phenomenon during flat film casting," International Journal of Heat and Mass Transfer 111, 1296-1313 (2017).
22. J. Drabek, M. Zatloukal, "Meltblown technology for production of polymeric microfibers/nanofibers: A review," Physics of Fluids 31 (9), art. no. 091301 (2019).
23. J. Drabek, M. Zatloukal, "Influence of long chain branching on fiber diameter distribution for polypropylene nonwovens produced by melt blown process," Journal of Rheology 63 (4), 519-532 (2019).
24. J. Drabek, M. Zatloukal, "Influence of molecular weight, temperature and extensional rheology on melt blowing process stability for linear isotactic polypropylene," Physics of Fluids 32 (8), 083110 (2020).

Table 1 Three principal invariants of the deformation rate tensor *D* and the objective velocity gradient $\bar{L}$.

	Simple shear flow	Uniaxial extensional flow	Equibiaxial flow	Planar flow
D	$\begin{pmatrix} 0 & \dot{\gamma}/2 & 0 \\ \dot{\gamma}/2 & 0 & 0 \\ 0 & 0 & 0 \end{pmatrix}$	$\begin{pmatrix} \dot{\varepsilon} & 0 & 0 \\ 0 & -\dot{\varepsilon}/2 & 0 \\ 0 & 0 & -\dot{\varepsilon}/2 \end{pmatrix}$	$\begin{pmatrix} \dot{\varepsilon} & 0 & 0 \\ 0 & \dot{\varepsilon} & 0 \\ 0 & 0 & -2\dot{\varepsilon} \end{pmatrix}$	$\begin{pmatrix} \dot{\varepsilon} & 0 & 0 \\ 0 & 0 & 0 \\ 0 & 0 & -\dot{\varepsilon} \end{pmatrix}$
$\bar{\mathrm{L}} = \mathrm{L}$	$\begin{pmatrix} 0 & \dot{\gamma} & 0 \\ 0 & 0 & 0 \\ 0 & 0 & 0 \end{pmatrix}$	$\begin{pmatrix} \dot{\varepsilon} & 0 & 0 \\ 0 & -\dot{\varepsilon}/2 & 0 \\ 0 & 0 & -\dot{\varepsilon}/2 \end{pmatrix}$	$\begin{pmatrix} \dot{\varepsilon} & 0 & 0 \\ 0 & \dot{\varepsilon} & 0 \\ 0 & 0 & -2\dot{\varepsilon} \end{pmatrix}$	$\begin{pmatrix} \dot{\varepsilon} & 0 & 0 \\ 0 & 0 & 0 \\ 0 & 0 & -\dot{\varepsilon} \end{pmatrix}$
$\mathrm{I}_\mathrm{D} = \mathrm{I}_{\bar{\mathrm{L}}}$	0	0	0	0
II_D	$\dot{\gamma}^2$	$3\dot{\varepsilon}^2$	$12\dot{\varepsilon}^2$	$4\dot{\varepsilon}^2$
$\mathrm{II}_{\bar{\mathrm{L}}}$	0	$3\dot{\varepsilon}^2$	$12\dot{\varepsilon}^2$	$4\dot{\varepsilon}^2$
$\mathrm{III}_\mathrm{D} = \mathrm{III}_{\bar{\mathrm{L}}}$	0	$\frac{1}{4}\dot{\varepsilon}^3$	$-2\dot{\varepsilon}^3$	0

Here, $\dot{\gamma}$ and $\dot{\varepsilon}$ represent shear and extensional strain rates, respectively.

Table 2 Three principal invariants of the deformation rate tensor *D* and the objective velocity gradient $\bar{L}$ in the mixed flows.

	Shear flow + uniaxial extensional flow	Shear flow + equibiaxial flow	Shear flow + planar flow
D	$\begin{pmatrix} \dot{\varepsilon} & \dot{\gamma}/2 & 0 \\ \dot{\gamma}/2 & -\dot{\varepsilon}/2 & 0 \\ 0 & 0 & -\dot{\varepsilon}/2 \end{pmatrix}$	$\begin{pmatrix} \dot{\varepsilon} & \dot{\gamma}/2 & 0 \\ \dot{\gamma}/2 & \dot{\varepsilon} & 0 \\ 0 & 0 & -2\dot{\varepsilon} \end{pmatrix}$	$\begin{pmatrix} \dot{\varepsilon} & \dot{\gamma}/2 & 0 \\ \dot{\gamma}/2 & 0 & 0 \\ 0 & 0 & -\dot{\varepsilon} \end{pmatrix}$
$\bar{\mathrm{L}} = \mathrm{L}$	$\begin{pmatrix} \dot{\varepsilon} & \dot{\gamma} & 0 \\ 0 & -\dot{\varepsilon}/2 & 0 \\ 0 & 0 & -\dot{\varepsilon}/2 \end{pmatrix}$	$\begin{pmatrix} \dot{\varepsilon} & \dot{\gamma} & 0 \\ 0 & \dot{\varepsilon} & 0 \\ 0 & 0 & -2\dot{\varepsilon} \end{pmatrix}$	$\begin{pmatrix} \dot{\varepsilon} & \dot{\gamma} & 0 \\ 0 & 0 & 0 \\ 0 & 0 & -\dot{\varepsilon} \end{pmatrix}$
$\mathrm{I}_{\mathrm{D}} = \mathrm{I}_{\bar{\mathrm{L}}}$	0	0	0
II_{D}	$3\dot{\varepsilon}^2 + \dot{\gamma}^2$	$12\dot{\varepsilon}^2 + \dot{\gamma}^2$	$4\dot{\varepsilon}^2 + \dot{\gamma}^2$
$\mathrm{II}_{\bar{\mathrm{L}}}$	$3\dot{\varepsilon}^2$	$12\dot{\varepsilon}^2$	$4\dot{\varepsilon}^2$
$\mathrm{III}_{\mathrm{D}}$	$\frac{1}{4}\dot{\varepsilon}^3 + \frac{1}{8}\dot{\gamma}^2\dot{\varepsilon}$	$-2\dot{\varepsilon}^3 + \frac{1}{2}\dot{\gamma}^2\dot{\varepsilon}$	$\frac{\dot{\gamma}^2\dot{\varepsilon}}{4}$
$\mathrm{III}_{\bar{\mathrm{L}}}$	$\frac{1}{4}\dot{\varepsilon}^3$	$-2\dot{\varepsilon}^3$	0

Here, $\dot{\gamma}$ and $\dot{\varepsilon}$ represent shear and extensional strain rates, respectively.

Table 3 Parameters of the GNF model for LDPE1 (T=140ºC), LDPE2 (T=150ºC) and LDPE3 (T=160ºC). A=10^{-8} Pa.s for all samples.

Sample name	η_0 (Pa.s)	λ_1 (s)	a (-)	n (-)	λ_2 (s)	β (-)	ζ (-)	ψ (-)
LDPE1 (high strain hardening)	3266.4	0.0933	0.7696	10^{-6}	$507.9532*10^{-4}$	$1.7149*10^{-2}$	$24.7119*10^{-3}$	35.5205
LDPE2 (medium strain hardening)	50829.6	8.4844	0.4904	10^{-6}	$1.7432*10^{-4}$	$9.3813*10^{-8}$	$16.0381*10^{-3}$	35.4614
LDPE3 (low strain hardening)	413830.6	23.0778	0.5124	0.1823	$12.1625*10^{-4}$	$1.1320*10^{-8}$	$7.4815*10^{-3}$	77.2106

Table 4 Parameters of the GNF model for metallocene high-density (mHDPE) and linear low-density (mLLDPE) polyethylenes with varying amounts of long-chain branches (LCBs) at 155ºC. A=10^{-8} Pa.s for all samples.

Sample name	η_0 (Pa.s)	λ_1 (s)	a (-)	n (-)	λ_2 (s)	β (-)	ζ (-)	ψ (-)
LCB-low mHDPE1	9687.5	2.2177	0.7571	0.6510	$501.5086*10^{-6}$	$9.2969*10^{-7}$	$2.3349*10^{-3}$	32.1062
LCB-medium mHDPE2	28481.6	9.3122	0.7738	0.5899	4.5913	$7.8399*10^{-4}$	$3.3020*10^{-3}$	73.2949
LCB-high mHDPE3	47948.3	2.6126	0.6179	0.3418	1.3166	$1.1719*10^{-3}$	$5.1234*10^{-3}$	127.2642
Linear mLLDPE1	11654.9	1.1682	1.5646	0.8291	$2.5161*10^{-7}$	$1.0314*10^{-7}$	$1.9825*10^{-3}$	0
LCB-low mLLDPE2	39440.6	1.5258	0.5333	0.4234	$3.1024*10^{-4}$	$5.8652*10^{-7}$	$3.8623*10^{-3}$	15.0290
LCB-high LLDPE3	32145.8	0.7586	0.5717	0.1698	$8.4339*10^{-4}$	$6.9952*10^{-6}$	$8.0257*10^{-3}$	24.2860

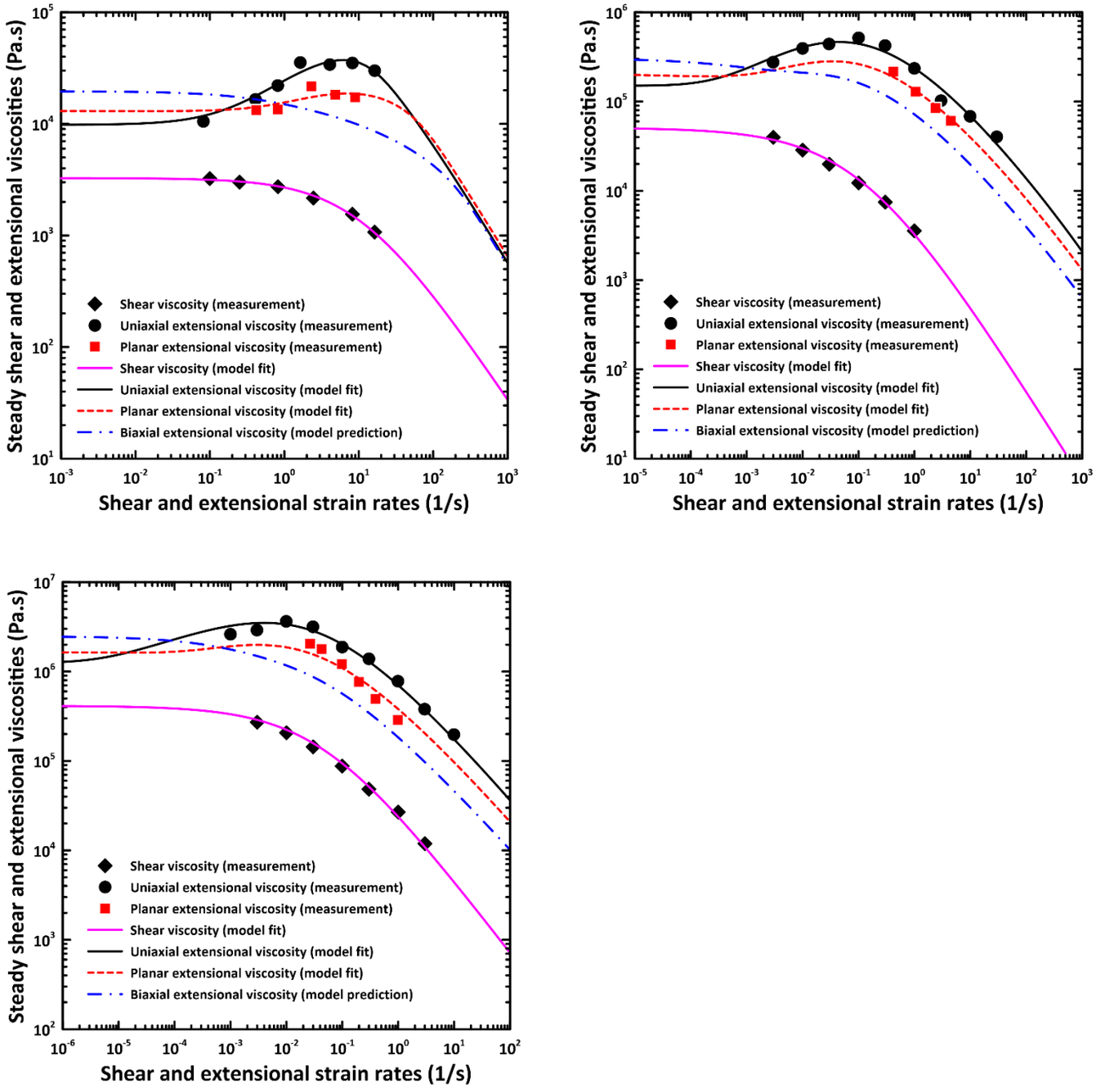

Figure 1 Comparison between the GNF model fits/prediction and the measured strain rate dependent shear and extensional viscosities for branched LDPE1 (left, top) LDPE2 (right, top) and LDPE3 (left, bottom). The measured data are taken from [15].

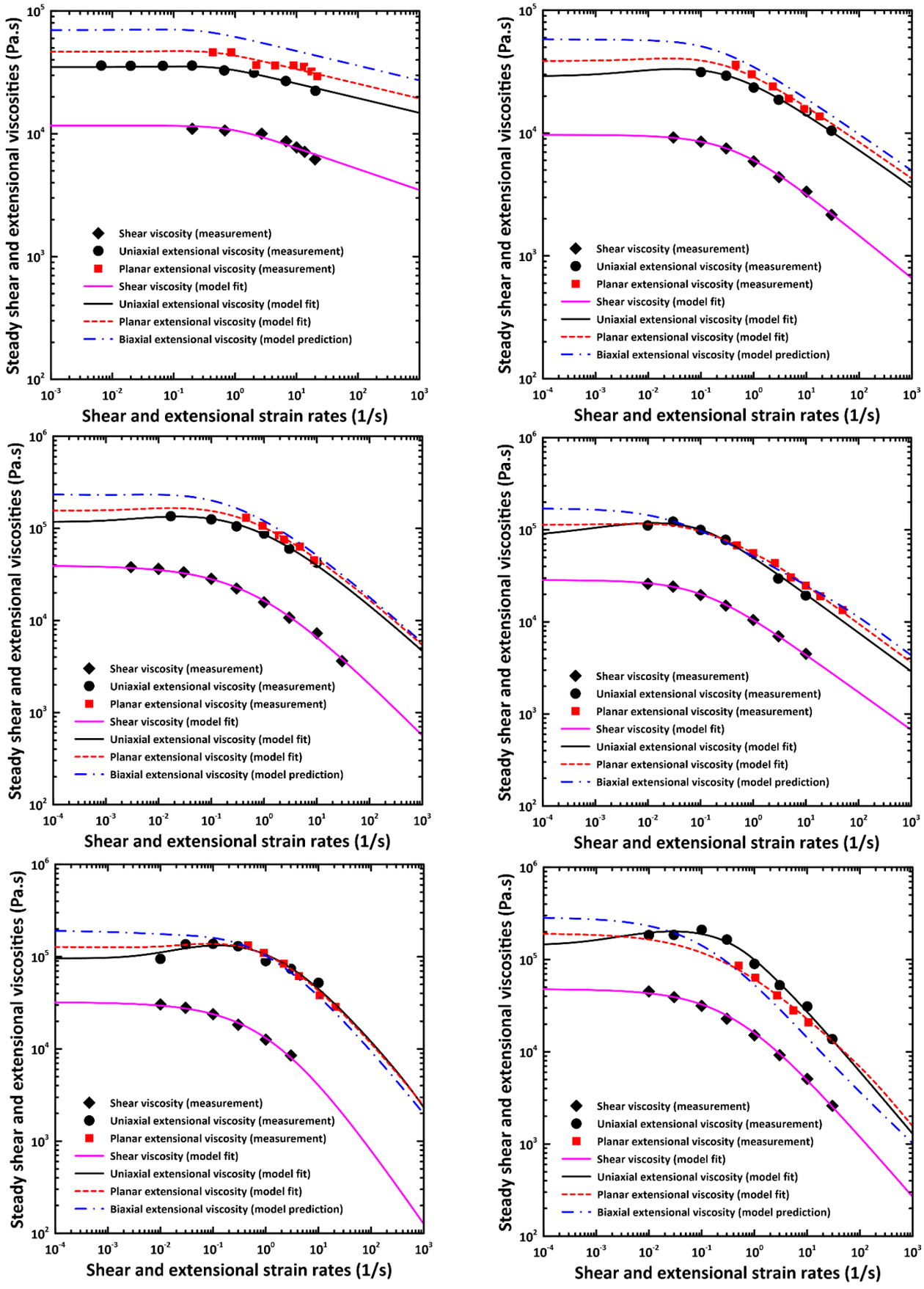

Figure 2 Comparison between the GNF model fits/prediction and the measured strain rate dependent shear and extensional viscosities for linear mLLDPE1 (left, top), slightly branched mLLDPE2 (left, in the middle), highly branched mLLDPE3 (left, bottom), slightly branched mHDPE1 (right, top), mHDPE2 medium branched (right, in the middle) and highly branched mHDPE3 (right, bottom). The measured data are taken from [15].

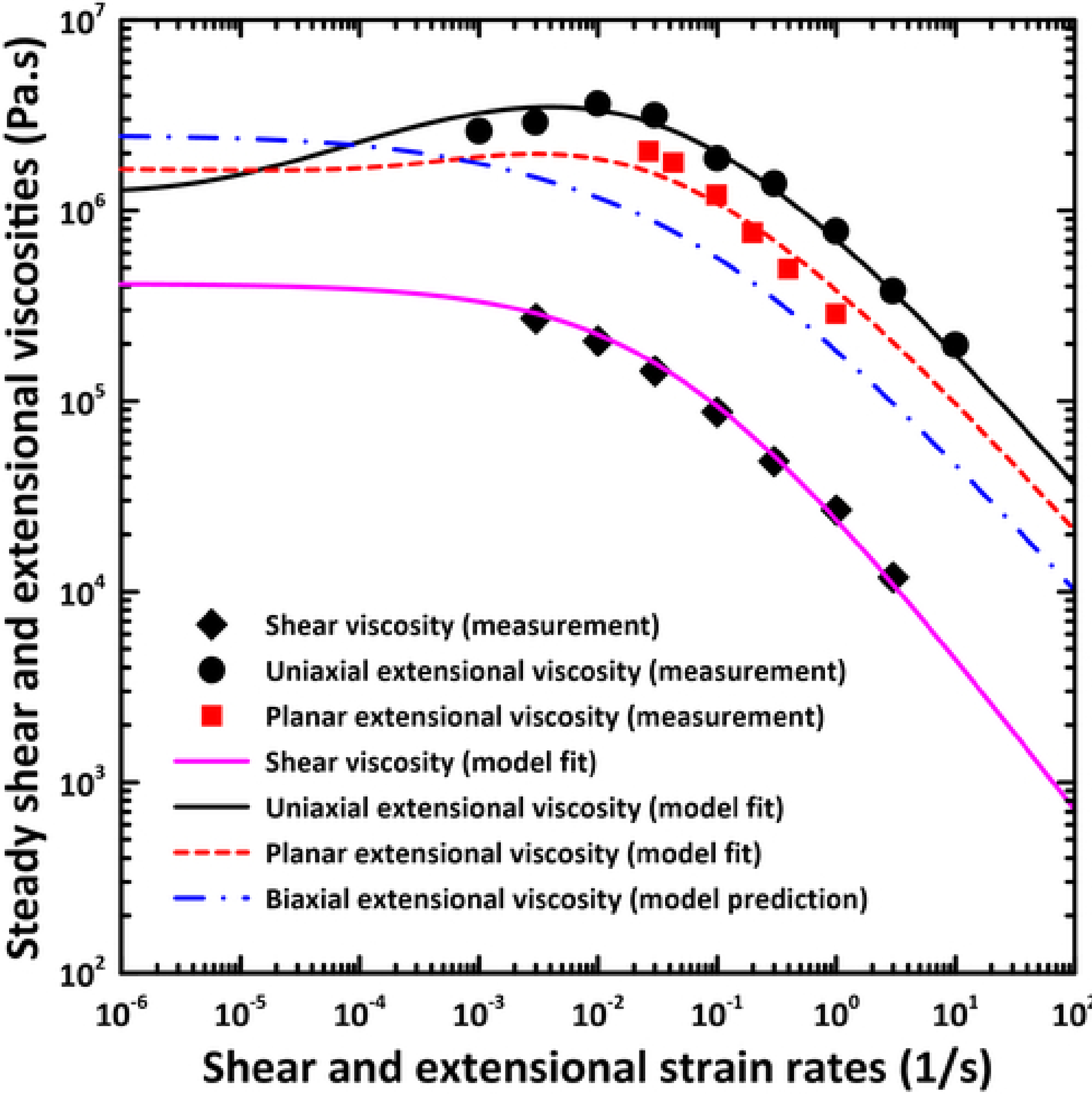
Steady shear and extensional viscosities (Pa.s)
10^7
10^6
10^5
10^4
10^3
10^2
Shear viscosity (measurement)
Uniaxial extensional viscosity (measurement)
Planar extensional viscosity (measurement)
Shear viscosity (model fit)
Uniaxial extensional viscosity (model fit)
Planar extensional viscosity (model fit)
Biaxial extensional viscosity (model prediction)
10^{-6}
10^{-5}
10^{-4}
10^{-3}
10^{-2}
10^{-1}
10^{0}
10^{1}
10^{2}
Shear and extensional strain rates (1/s)

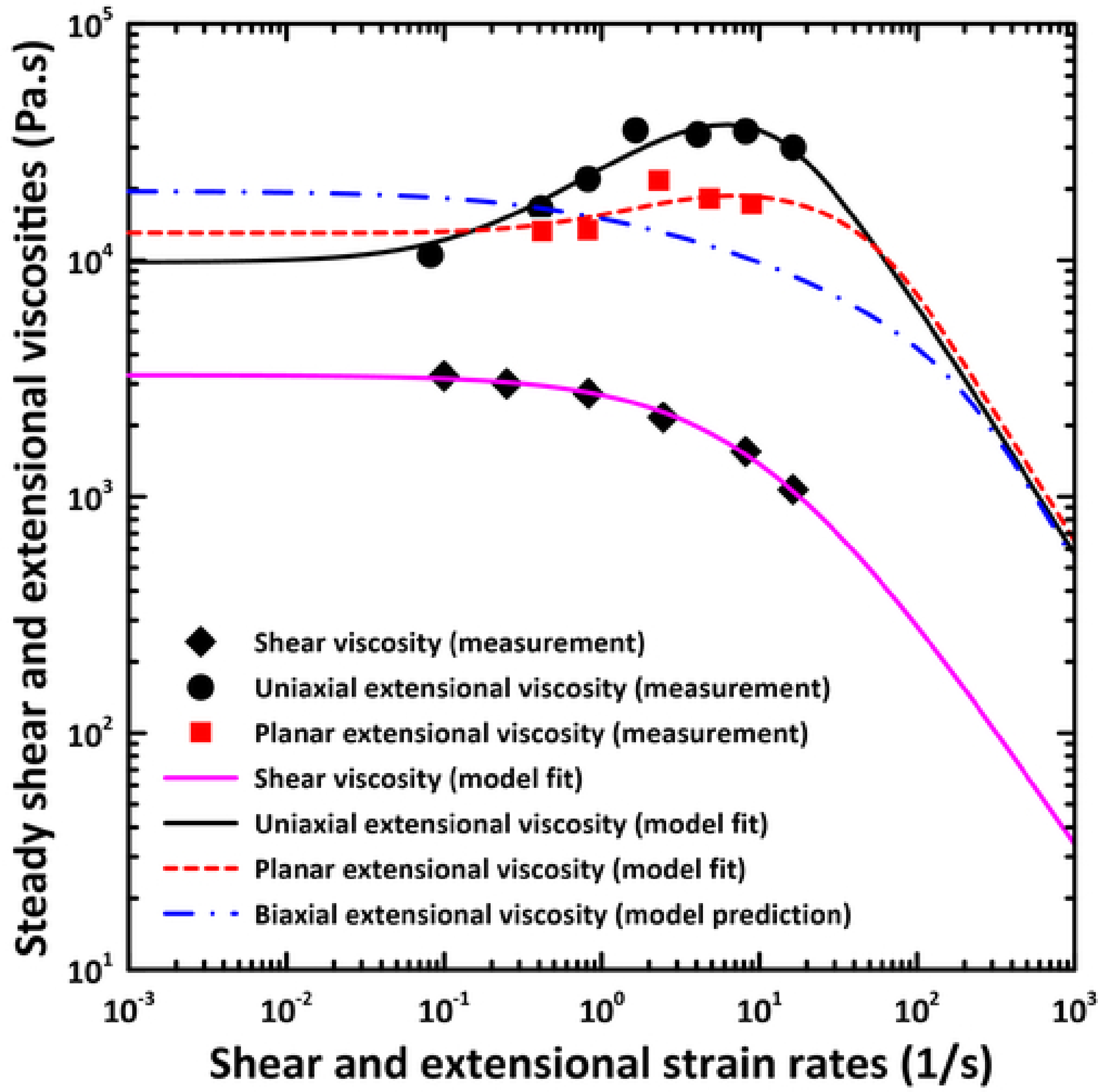
Steady shear and extensional viscosities (Pa.s)
10^5
10^4
10^3
10^2
10^1
10^{-3}
10^{-2}
10^{-1}
10^0
10^1
10^2
10^3
Shear and extensional strain rates (1/s)
Shear viscosity (measurement)
Uniaxial extensional viscosity (measurement)
Planar extensional viscosity (measurement)
Shear viscosity (model fit)
Uniaxial extensional viscosity (model fit)
Planar extensional viscosity (model fit)
Biaxial extensional viscosity (model prediction)

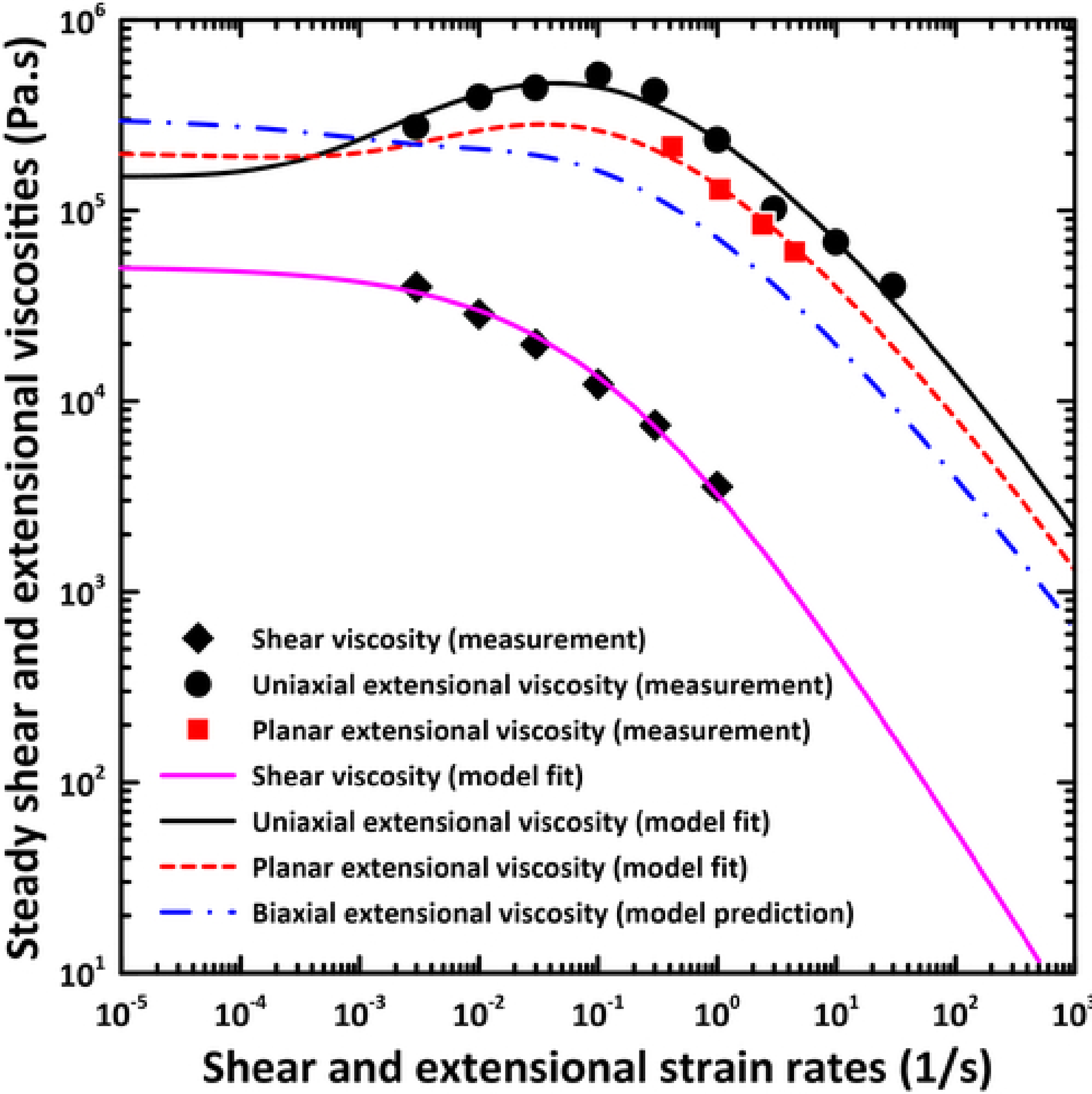
Steady shear and extensional viscosities (Pa.s)
Shear and extensional strain rates (1/s)
Shear viscosity (measurement)
Uniaxial extensional viscosity (measurement)
Planar extensional viscosity (measurement)
Shear viscosity (model fit)
Uniaxial extensional viscosity (model fit)
Planar extensional viscosity (model fit)
Biaxial extensional viscosity (model prediction)

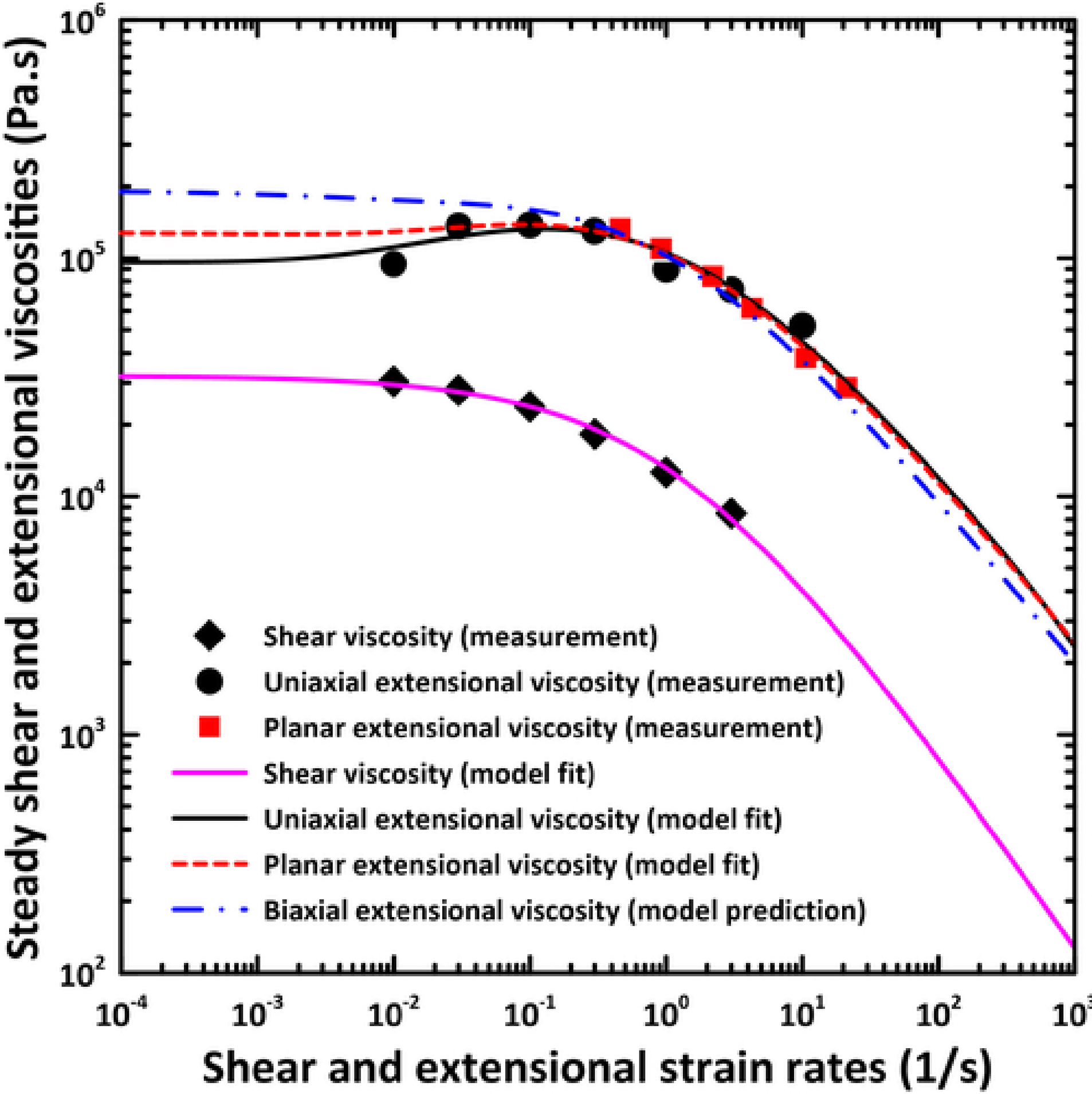
Steady shear and extensional viscosities (Pa.s)
10^6
10^5
10^4
10^3
10^2
10^{-4}
10^{-3}
10^{-2}
10^{-1}
10^0
10^1
10^2
10^3
Shear and extensional strain rates (1/s)
Shear viscosity (measurement)
Uniaxial extensional viscosity (measurement)
Planar extensional viscosity (measurement)
Shear viscosity (model fit)
Uniaxial extensional viscosity (model fit)
Planar extensional viscosity (model fit)
Biaxial extensional viscosity (model prediction)

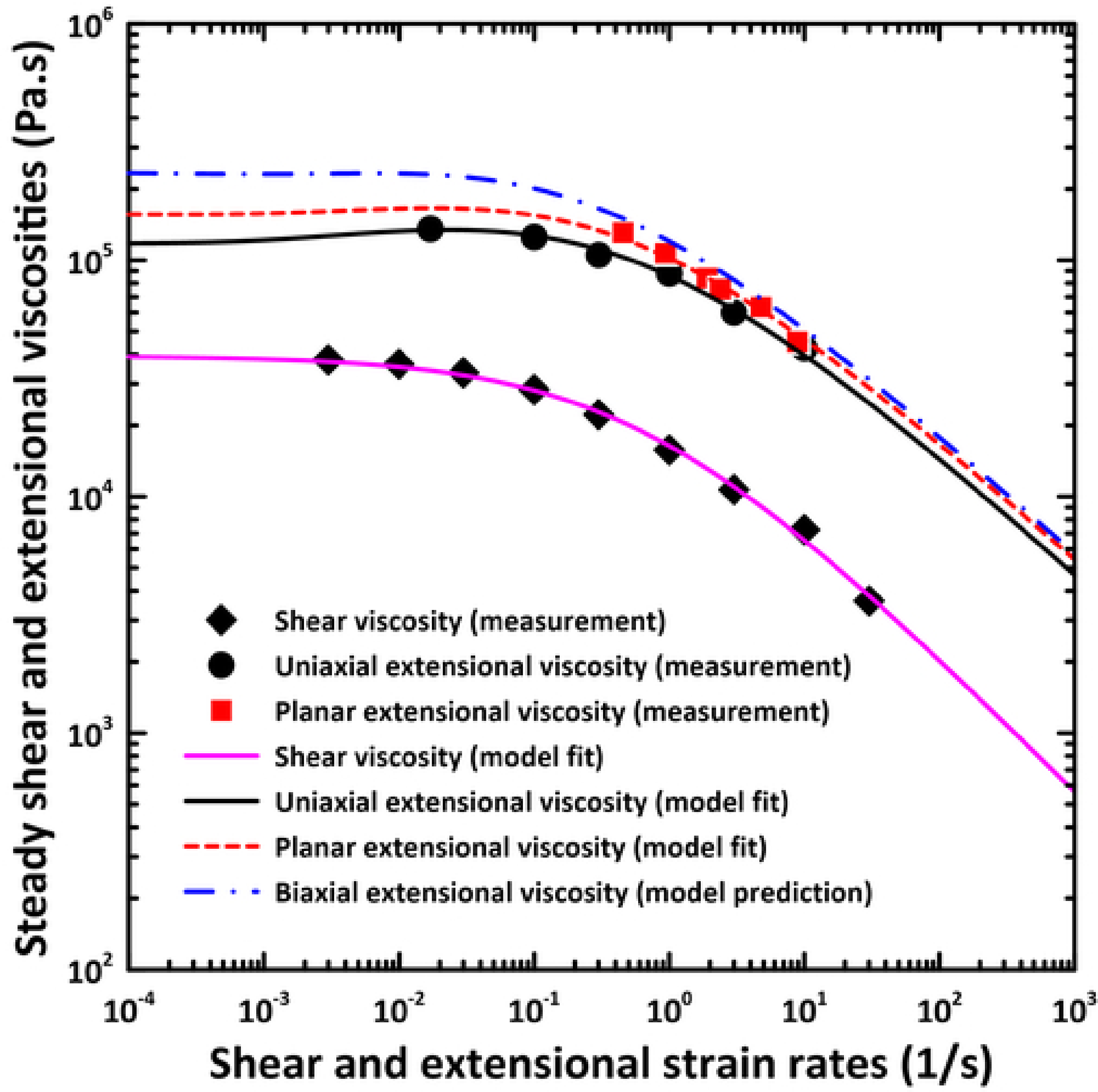
Steady shear and extensional viscosities (Pa.s)
10^6
10^5
10^4
10^3
10^2
10^{-4}
10^{-3}
10^{-2}
10^{-1}
10^0
10^1
10^2
10^3
Shear and extensional strain rates (1/s)
Shear viscosity (measurement)
Uniaxial extensional viscosity (measurement)
Planar extensional viscosity (measurement)
Shear viscosity (model fit)
Uniaxial extensional viscosity (model fit)
Planar extensional viscosity (model fit)
Biaxial extensional viscosity (model prediction)

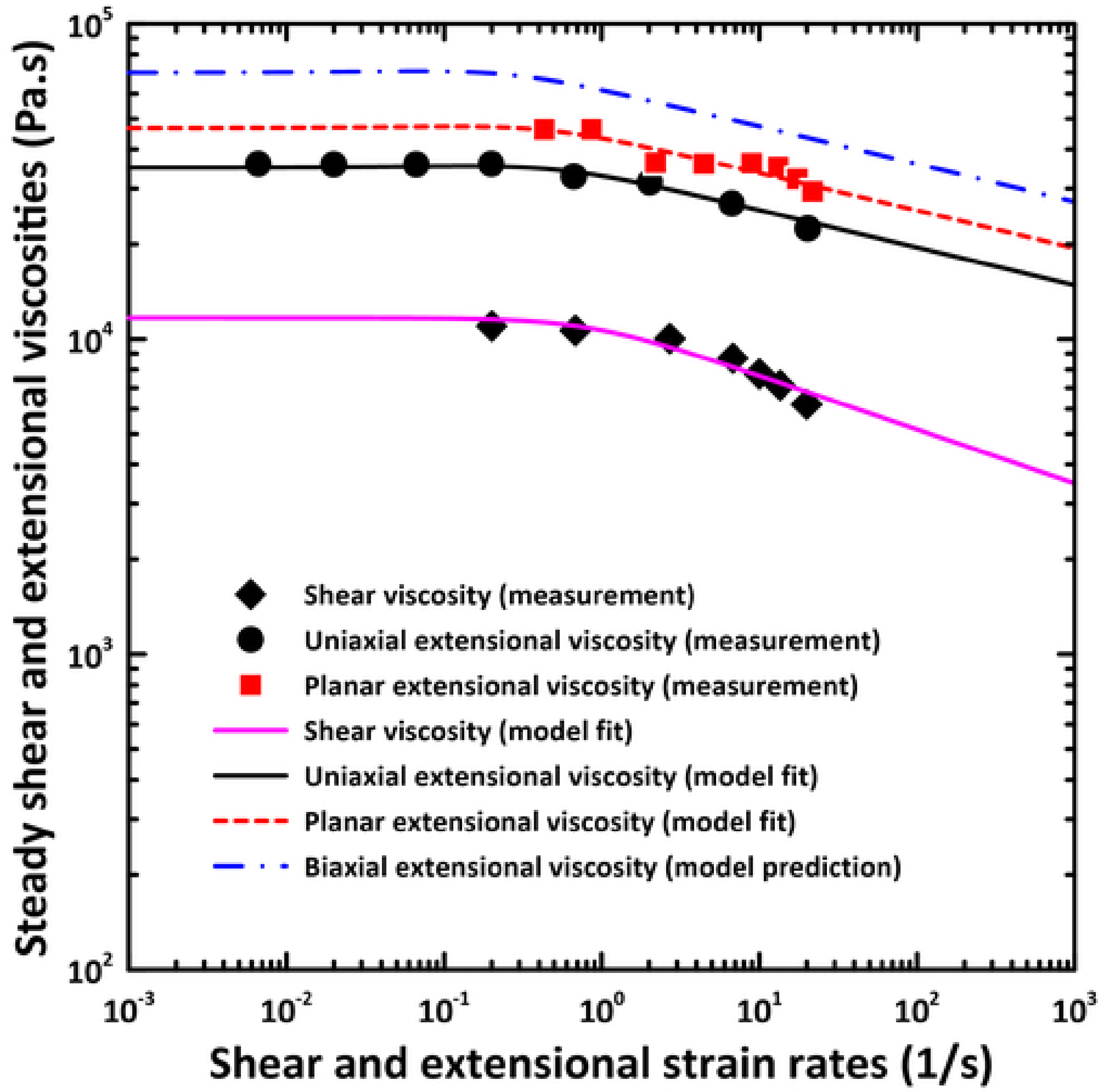
Steady shear and extensional viscosities (Pa.s)
10^5
10^4
10^3
10^2
10^{-3}
10^{-2}
10^{-1}
10^0
10^1
10^2
10^3
Shear and extensional strain rates (1/s)
Shear viscosity (measurement)
Uniaxial extensional viscosity (measurement)
Planar extensional viscosity (measurement)
Shear viscosity (model fit)
Uniaxial extensional viscosity (model fit)
Planar extensional viscosity (model fit)
Biaxial extensional viscosity (model prediction)

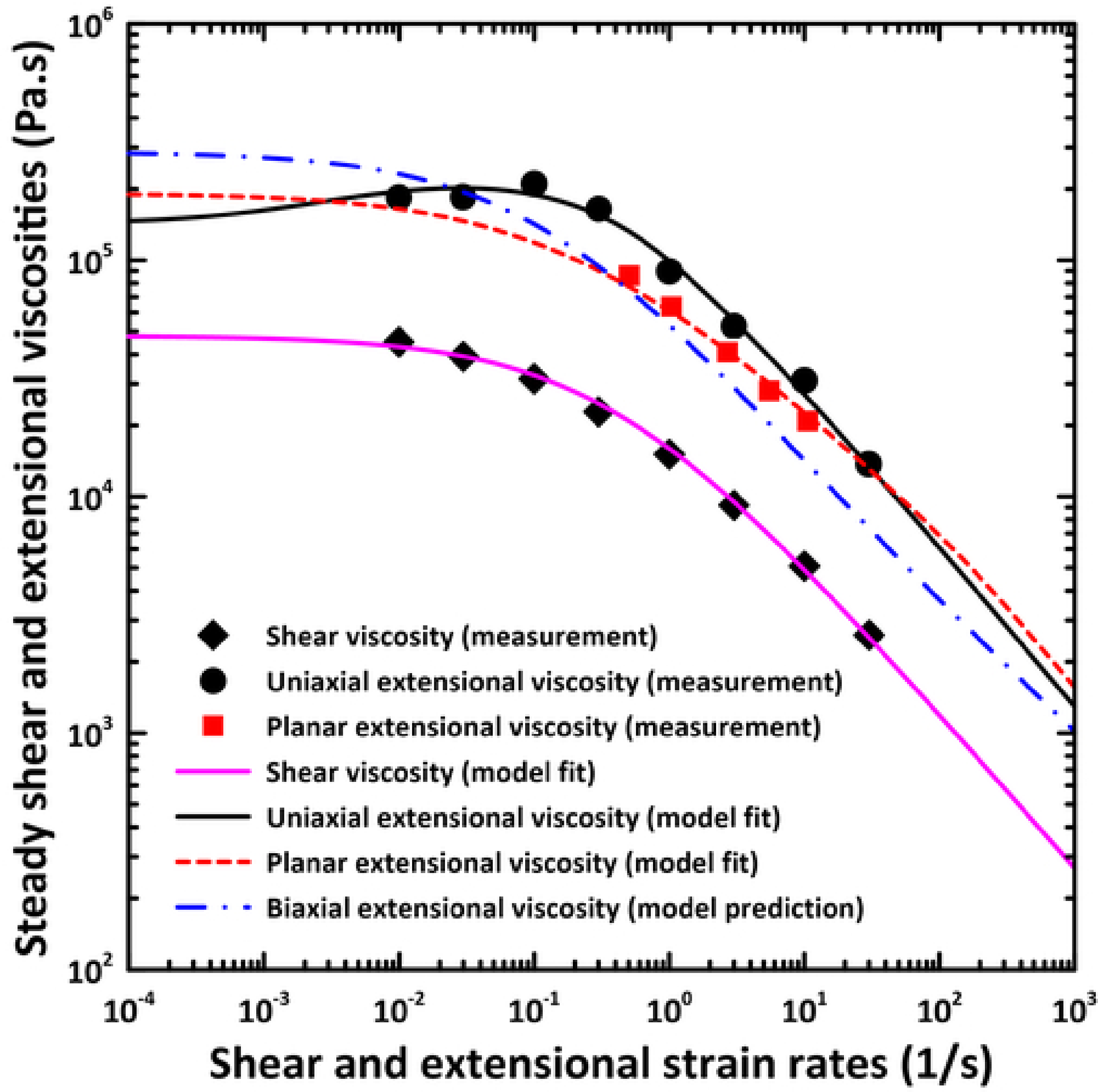
Steady shear and extensional viscosities (Pa.s)
10^6
10^5
10^4
10^3
10^2
10^{-4}
10^{-3}
10^{-2}
10^{-1}
10^0
10^1
10^2
10^3
Shear and extensional strain rates (1/s)
Shear viscosity (measurement)
Uniaxial extensional viscosity (measurement)
Planar extensional viscosity (measurement)
Shear viscosity (model fit)
Uniaxial extensional viscosity (model fit)
Planar extensional viscosity (model fit)
Biaxial extensional viscosity (model prediction)

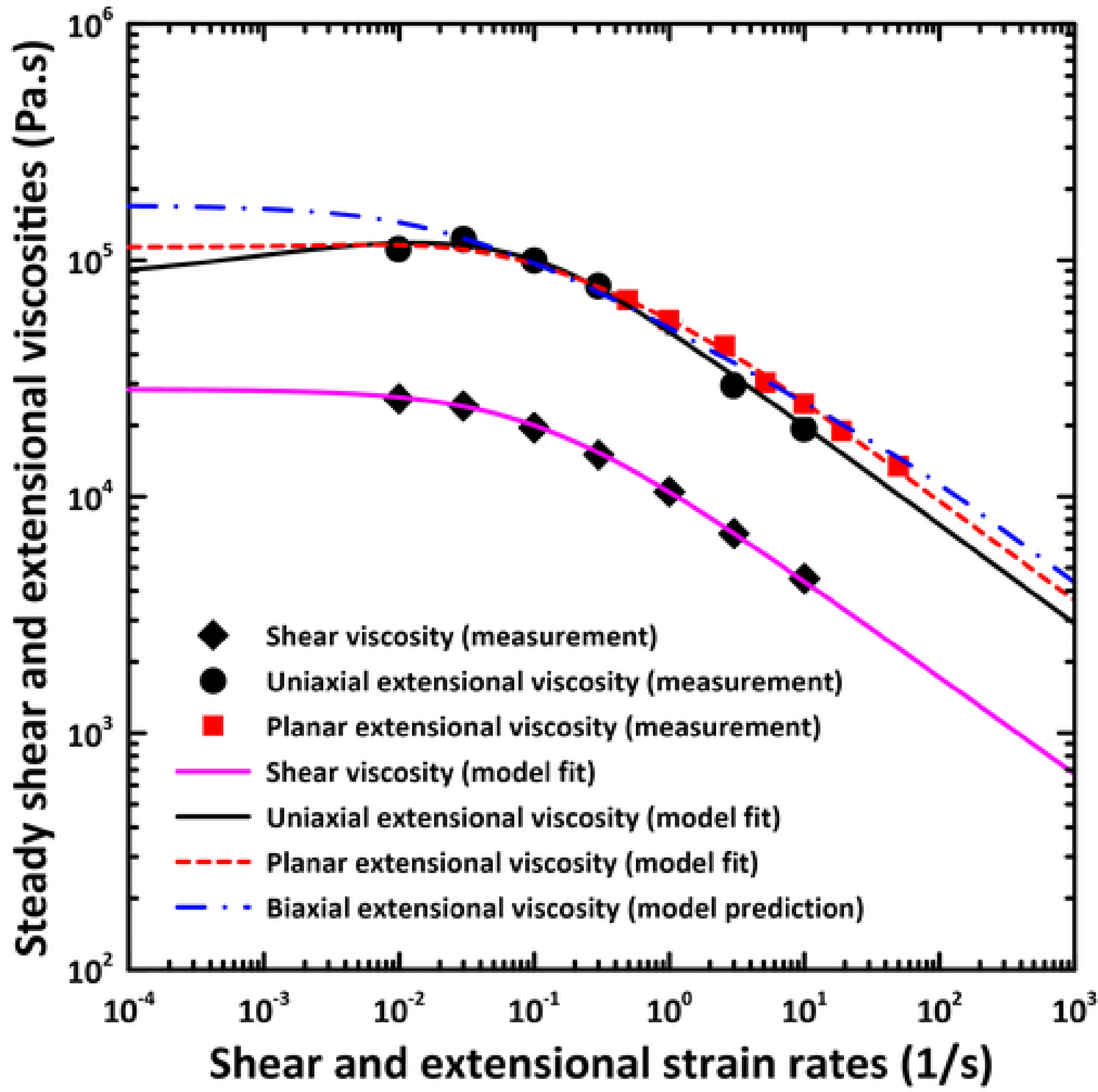
Steady shear and extensional viscosities (Pa.s)
10^6
10^5
10^4
10^3
10^2
10^{-4}
10^{-3}
10^{-2}
10^{-1}
10^0
10^1
10^2
10^3
Shear and extensional strain rates (1/s)
Shear viscosity (measurement)
Uniaxial extensional viscosity (measurement)
Planar extensional viscosity (measurement)
Shear viscosity (model fit)
Uniaxial extensional viscosity (model fit)
Planar extensional viscosity (model fit)
Biaxial extensional viscosity (model prediction)

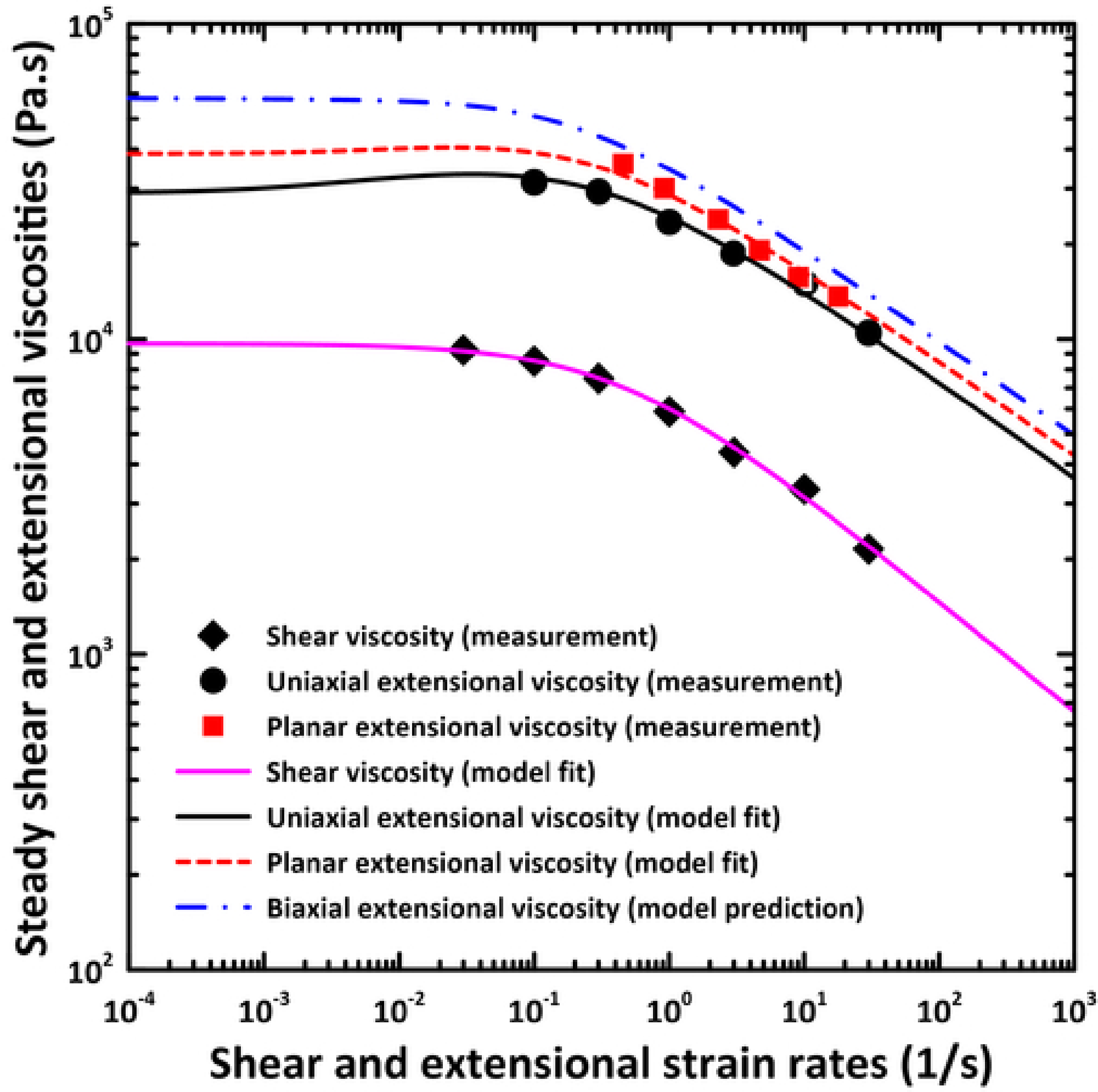
Steady shear and extensional viscosities (Pa.s)
10^5
10^4
10^3
10^2
10^{-4}
10^{-3}
10^{-2}
10^{-1}
10^0
10^1
10^2
10^3
Shear and extensional strain rates (1/s)
Shear viscosity (measurement)
Uniaxial extensional viscosity (measurement)
Planar extensional viscosity (measurement)
Shear viscosity (model fit)
Uniaxial extensional viscosity (model fit)
Planar extensional viscosity (model fit)
Biaxial extensional viscosity (model prediction)